Ecological Modelling 328 (2016) 136–147

Contents lists available at ScienceDirect

Ecological Modelling

journal homepage: www.elsevier.com/locate/ecolmodel

A modeling study examining the impact of nutrient boundaries on primary production on the Louisiana continental shelf

James J. Pauer[a,*], Timothy J. Feist[b], Amy M. Anstead[c], Phillip A. DePetro[c], Wilson Melendez[d], John C. Lehrter[e], Michael C. Murrell[e], Xiaomi Zhang[b], Dong S. Ko[f]

[a] U.S. Environmental Protection Agency, Office of Research and Development, National Health and Environmental Effects Research Laboratory, Mid-Continent Ecology Division, Large Lakes and Rivers Forecasting Research Branch, Large Lakes Research Station, 9311 Groh Road, Grosse Ile, MI 48138, USA
[b] Trinity Engineering Associates, Inc., Large Lakes Research Station, 9311 Groh Road, Grosse Ile, MI 48138, USA
[c] ICF International, Large Lakes Research Station, 9311 Groh Road, Grosse Ile, MI 48138, USA
[d] CSC Government Solutions LLC, a CSRA Company, Large Lakes Research Station, 9311 Groh Road, Grosse Ile, MI 48138, USA
[e] U.S. Environmental Protection Agency, Office of Research and Development, National Health and Environmental Effects Research Laboratory, Gulf Ecology Division, 1 Sabine Island Drive, Gulf Breeze, FL 32561, USA
[f] US Naval Research Laboratory, Stennis Space Center, MS 39529, USA

ARTICLE INFO

Article history:
Received 21 September 2015
Received in revised form 10 February 2016
Accepted 13 February 2016

Keywords:
Numerical model
Louisiana continental shelf (LCS)
Primary production
Nutrients
Boundary concentrations
Co-limitation

ABSTRACT

Nutrient inputs to the Louisiana continental shelf (LCS) from lateral ocean boundaries can be significant, but the effect of these nutrients on LCS primary production has not been examined. Herein, we apply a three-dimensional physical-biogeochemical model to calculate nitrogen and phosphorus mass balances on the LCS and quantify the contributions of riverine and offshore nutrient inputs to primary production. A model sensitivity analysis to different offshore nutrient concentrations indicated that modeled primary production was most sensitive to boundary nitrogen concentrations, whereas changing boundary phosphorus concentrations had little effect. The primary production response also varied spatially and temporally, with its greatest response being to changing boundary nitrogen concentrations in areas furthest from the river plume, and during the late summer for all regions of the shelf when Mississippi River discharge approaches its annual minimum. These results indicate that even for river-dominated shelves like the LCS, uncertain boundary condition nutrient concentrations are likely to contribute significantly to uncertainty in modeled primary production. The modeling study highlights the need for further observational studies to understand the sources and variability of nutrients at LCS offshore boundaries and the impacts to LCS primary production.

Published by Elsevier B.V.

1. Introduction

Large seasonal discharges of nitrogen and phosphorus from the Mississippi-Atchafalaya River Basin (MARB) stimulate phytoplankton growth and accrual of phytoplankton derived organic matter on the inner Louisiana continental shelf (LCS) (Lohrenz et al., 2008; Le et al., 2014; Fry et al., 2015), which contributes to hypoxia in this system (Rabalais et al., 2002; Bianchi et al., 2010). While Mississippi River loadings to the northern Gulf of Mexico have been measured over several decades (United States Geological Survey, 2013; Battaglin et al., 2010; Aulenbach et al., 2007), much less is known about the nutrient loads flowing across the open shelf boundaries. These boundary inflows and outflows of nutrients can represent a significant source or sink for the LCS (Walsh et al., 1989; Sahl et al., 1993; Lehrter et al., 2013) and may support primary production on the middle and outer shelf (Chen et al., 2000; Lehrter et al., 2009).

Further, whereas primary production in the river plume of the LCS is correlated with river nutrient loads (Lohrenz et al., 2008), primary production in non-plume regions of the shelf is not positively correlated with river loads (Lehrter et al., 2009). These observations have led to speculation that non-river nutrient sources may be important for fueling primary production away from the river plumes and during periods of low river discharge (Chen et al., 2000). Thus, quantifying the significance of the non-river nutrient inputs to phytoplankton production is important for teasing out the impacts of land-based nutrients on this system and for elucidating the factors contributing to primary production dynamics.

* Corresponding author. Tel.: +1 734 692 7635; fax: +1 734 692 7603.
E-mail address: pauer.james@epa.gov (J.J. Pauer).

http://dx.doi.org/10.1016/j.ecolmodel.2016.02.007
0304-3800/Published by Elsevier B.V.

Numerical ecosystem models have proven useful for understanding the relationships between river nutrient loads and primary production on the LCS. Bierman et al. (1994) demonstrated the importance of river nutrients and light availability on the spatial and temporal distribution of phytoplankton biomass. Green et al. (2008) explored the role of nitrogen limitation in regulating primary production in the river plume, and a key conclusion was that physical dilution of river nitrate due to mixing with offshore surface water is one of the main regulators of the amount of primary production. Fennel et al. (2011) and Laurent and Fennel (2014) have also examined the roles of nitrogen and phosphorus limitation on the LCS. In all of these studies, lower nutrient concentrations resulted in less primary production and thus a reduction in the sedimentation of organic matter to the benthos. However, the potential contribution of boundary condition nutrient inflows to the shelf nutrient regime and primary production has not yet been evaluated.

In this study, we have applied a three-dimensional physical-biogeochemical model to quantify and compare the contribution of shelf boundary nutrient fluxes and river nutrient loads to LCS nutrient concentrations and primary production. The main conclusion is that the modeled nutrient concentrations and production were sensitive to changes in nutrient boundary conditions. Thus, model uncertainty due to the lack of spatial and temporal understanding of boundary nutrient dynamics is significant.

2. Methods

2.1. Model description

The Gulf of Mexico Dissolved Oxygen Model (GoMDOM) is a process-based numerical model of the northern Gulf of Mexico. The model domain encompasses the LCS and a small area east of the Mississippi River delta (Fig. 1). The model grid has an approximately 6 km by 6 km horizontal resolution and 26 vertical sigma layers. The sigma layer fractions range from 0.01 to 0.04, with higher resolution at the top two sigma layers to better account for wind and heat effects.

GoMDOM has 19 state variables: diatoms and non-diatoms phytoplankton groups; one zooplankton grazer; labile and refractory particulate organic carbon; labile and refractory particulate organic phosphorus and labile and refractory particulate organic nitrogen; dissolved organic carbon, dissolved organic phosphorus and dissolved organic nitrogen; biogenic and dissolved silica; soluble reactive phosphorus; ammonium; nitrate + nitrite; dissolved oxygen and salinity. The kinetics equations used in GoMDOM are based on the LM3-Eutro eutrophication model that was applied to Lake Michigan (Pauer et al., 2008, 2011; Melendez et al., 2009). Several new features, as described below, were made to the LM3-Eutro kinetics, namely adding dissolved oxygen as a state variable, changing the sediment equations, and improving the representation of the zooplankton and light formulations. A one-dimensional variation of this model, GoMDOM-1D, has been applied to a number of sites on the LCS (Pauer et al., 2014).

2.2. Dissolved oxygen

Dissolved oxygen was not included in the original LM3-Eutro model, but was added as a state variable in GoMDOM. Sources of dissolved oxygen are photosynthesis and exchange with the atmosphere (reaeration), while algal and zooplankton respiration, dissolved organic carbon oxidation, nitrification and sediment oxygen demand are oxygen sinks. Detailed equations used to describe these sources and sinks can be found in Pauer et al. (2014).

2.3. Zooplankton

The zooplankton mortality formulation used in the original LM3-Eutro model was replaced with a quadratic dependency on the zooplankton concentration to simulate predation by higher trophic levels (Banas et al., 2009; Cerco and Meyers, 2000). As noted by Cerco and Noel (2004), the use of a quadratic dependence reduces the phytoplankton–zooplankton biomass oscillations, providing a higher degree of stability to the phytoplankton standing crop.

2.4. Sediment fluxes

Sediment nitrate fluxes and sediment oxygen demand (SOD) were modeled using relationships developed by Lehrter et al.

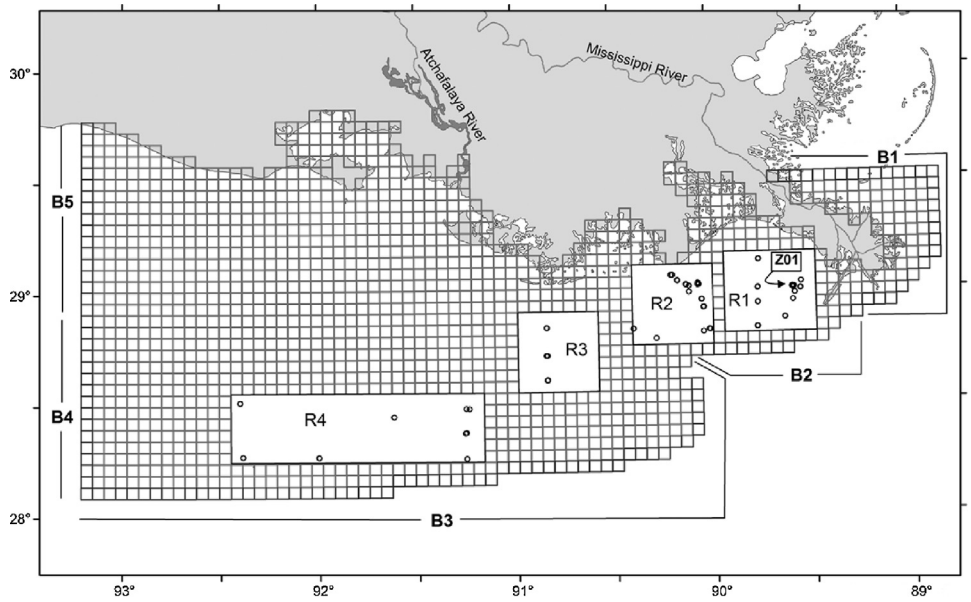

Fig. 1. The Louisiana continental shelf of the northern Gulf of Mexico study area showing the GoMDOM computational grid, the spatial regions with the sampling stations, and the boundaries. The four spatial regions are the Mississippi Plume (region 1, R1), Mississippi Intermediate (region 2, R2), River Transition (region 3, R3) and Outer Continental Shelf (region 4, R4). The five boundaries are Eastern (B1), Trench (B2), Offshore (B3), Outer western (B4) and Inner western (B5).

(2012) for the LCS of the Gulf of Mexico. The nitrogen flux formulation is shown in Eq. (1),

$$(NO_x)_{\text{flux}} = 0.0057C_{DO} - 0.5235 \quad (1)$$

where $(NO_x)_{\text{flux}}$ is the nitrate + nitrite flux (mmol m^{-2} d^{-1}) and C_{DO} is the dissolved oxygen concentration in the bottom sigma layer (mmol m^{-3}). SOD was modeled as a function of bottom layer dissolved oxygen concentration and temperature based on empirical relationships of these variables with SOD (Murrell and Lehrter, 2011; Lehrter et al., 2012, Lehrter unpublished data, R-squared = 0.59; n = 43) assuming the temperature coefficient, Q_{10} = 2.

$$\text{SOD} = (0.1215C_{DO} - 9.236 \times 10^{-5})\,2^{(T-T_{ref})/10} \quad (2)$$

where SOD is sediment oxygen demand (kg O_2 m^{-2} d^{-1}), C_{DO} is dissolved oxygen concentration (kg m^{-3}), T is temperature (°C), and T_{ref} is the reference temperature of 25 °C.

2.5. Light and phytoplankton growth

An empirical equation was used to estimate the attenuation of light within the water column and to calculate the light attenuation coefficients for each model cell. The development of this equation, which is based on pairing measured light profiles and water column characteristics, is described in Appendix 1. The average light (PAR) at the subsurface layers (I_{ave}, μmol quanta m^{-2} s^{-1}) was subsequently calculated using Beer's Law (Eq. (3)),

$$I_{ave} = \frac{I_s}{k_d \Delta z}\left[e^{-k_d z_1} - e^{-k_d z_2}\right] \quad (3)$$

where I_s is the photosynthetically active radiation (PAR, μmol quanta m^{-2} s^{-1}) at the water surface, ΔZ (meters) is distance from surface (Z_1) to bottom (Z_2) of the cell, and k_d is the calculated light attenuation coefficient (m^{-1}).

The Jassby and Platt (1976) equation was rearranged to determine the light limitation coefficient factor, $f(I)$, based on the photosynthesis-irradiation relationship coefficients as shown in Eq. (4).

$$f(I) = \left(\frac{P^B}{P^B_{\max}}\right) = \tanh\left(\frac{\alpha^B I_{ave}}{P^B_{\max}}\right) \quad (4)$$

where P^B is the production rate (g C (g chla h)$^{-1}$), P^B_{max} is maximum production rate (g C (g chla h)$^{-1}$) and α^B is the initial slope of the photosynthesis-irradiance curve (g C (g chla h)$^{-1}$ (μmol quanta m^{-2} s^{-1})$^{-1}$).

3. Model input

3.1. Loadings

River nutrient loads entered the GoMDOM computational grid at 56 locations. Over 98% of the river loads that enter the model grid are from the MARB. United States Geological Survey (USGS) monthly loading estimates of nitrogen, phosphorus and silica for the Mississippi River at Saint Francisville, MS, and for the Atchafalaya River at Melville, LA (USGS, 2013; Battaglin et al., 2010; Aulenbach et al., 2007) were assigned to each river outlet, distributary or pass in the MARB based upon the percentage of total river flow represented by each outlet. Organic nitrogen concentrations were calculated as the difference between total Kjehdahl nitrogen and ammonia, with previous river sampling data used to split the organic nitrogen into dissolved (52% of organic nitrogen loads for Mississippi River outlets and 55% for Atchafalaya River outlets) and particulate (48% for Mississippi River outlets and 45% for Atchafalaya River outlets). Based upon available sampling data, dissolved organic phosphorus loads where set to 15% of soluble reactive phosphorus loads for Mississippi River outlets and 20% for Atchafalaya River outlets. Daily loads for the model were estimated by flow-weighting the monthly load estimates based upon daily river flow. Loads were distributed vertically at model cells were they entered by matching the vertical flow distribution, typically distributed among the first ten sigma layers. USGS loadings were not available for particulate and dissolved organic carbon, dissolved oxygen, dissolved organic phosphorus, or for tributaries outside the MARB. Estimates for the remaining daily loads were calculated by multiplying average monthly constituent concentrations for the specific river by the daily flow for that river. Observational data used for calculating these loads were obtained from the USGS National Water Information System (NWIS) site (http://www.waterdata.usgs.gov/nwis/qw, accessed 31.01.11) and from the U.S. EPA STORET database (http://www.epa.gov/storet/dbtop.html, accessed 31.01.11). If data were not available for a specific river and time period, data were used from a nearby similar river or from a similar time period. Rivers with missing data made up less than 2% of the total river loads entering the GoMDOM grid, so any errors from the loading assumptions were small. Based on an analysis of chlorophyll and POC data presented by Dagg et al. (2005) from the lower Mississippi River, we assume a conservative estimate of 10% of the POC enters the Gulf as phytoplankton, while the zooplankton loads were zero.

3.2. Atmospheric forcing: nutrient loads, wind and light

Atmospheric nitrogen loading data were generated by the Community Multiscale Air Quality (CMAQ) model output (Dennis, personal communication, Byun and Schere, 2006), which included monthly dry and wet deposition of oxidized (nitrate) and reduced (ammonium) nitrogen. The proportional area of each GoMDOM grid cell overlapped by each CMAQ grid cell was calculated to yield a monthly atmospheric nitrogen load for each model grid cell.

High resolution wind velocity measurements were obtained from the Coupled Ocean/Atmosphere Mesoscale Prediction System (COAMPS), a regional weather forecast model (Hodur, 1997). Comparisons of the model output to velocity measured at a sea buoy in the LCS indicated that the modeled winds accurately represented the winds at that location (Lehrter et al., 2013). Solar radiation data for the GoMDOM computational grid were obtained from the Navy Operational Global Atmospheric Prediction System (NOGAPS) with an approximately 50-km grid resolution (Rosmond et al., 2002) and on a 3-h interval. Nearest neighbor interpolation and a Zonal Statistics tool (ESRI, 2009) were used to calculate average wind speed and solar radiation values for each GoMDOM grid cell.

3.3. Field data used to calibrate the model, initial conditions and boundary conditions

A dataset of water-column hydrography and nutrients, primary production rates, and sediment nutrient fluxes was collected in the northern Gulf of Mexico during three cruises in April, June, and September of 2006 (Lehrter et al., 2009, 2012, 2013; Murrell et al., 2013a, 2013b). These observations were used to estimate boundary conditions and to compare with model results. A carbon to chlorophyll (C:chla) ratio of 50 mg C mg $chla^{-1}$ was used to calculate model phytoplankton carbon from field-measured chlorophyll, as in Pauer et al., 2014. Based on a study conducted by Rabalais et al. (2002) that found the majority of the phytoplankton biomass to consist of diatoms, we decided to set diatoms to be 90% of the phytoplankton carbon. Zooplankton carbon was calculated based on reported values for the Gulf of Mexico (Breed et al., 2004; Sutor and Dagg, 2008; Liu and Dagg, 2003; NMFS, 2005). Water-column primary production rates were calculated

Table 1a
Nitrogen boundary concentrations for the January to May (Jan–May), June to August (Jun–Aug) and September to December (Sep–Dec) periods for 2006. Dissolved inorganic nitrogen (DIN) and total nitrogen (TN) boundary concentration values (μg/L) are shown for the surface and bottom waters for the different boundaries.

	Jan–May		Jun–Aug		Sep–Dec	
	DIN	TN	DIN	TN	DIN	TN
Eastern surface	88.7	202.7	24.7	125.1	52.1	783.3
Eastern bottom	48.2	82.2	115.8	164.4	137.4	165.7
Trench surface	10.6	236.0	8.5	163.4	2.4	163.3
Trench bottom	33.3	194.6	84.8	162.3	120.8	214.6
Offshore surface	11.2	153.1	11.9	107.5	3.4	108.7
Offshore bottom	27.6	153.5	41.4	127.0	50.7	156.5
Inner western	15.1	154.0	18.4	220.0	10.1	193.9
Outer western	2.2	106.4	9.0	142.3	11.1	137.9

Table 1b
Phosphorus boundary concentrations for the January to May (Jan–May), June to August (Jun–Aug) and September to December (Sep–Dec) periods for 2006. Soluble reactive phosphorus (SRP) and total phosphorus (TP) boundary concentration values (μg/L) are shown for the surface and bottom waters for the different boundaries.

	Jan–May		Jun–Aug		Sep–Dec	
	SRP	TP	SRP	TP	SRP	TP
Eastern surface	7.9	13.7	5.4	9.1	8.7	22.2
Eastern bottom	8.5	29.6	16.7	29.7	17.3	26.9
Trench surface	1.8	17.2	1.7	16.2	5.4	15.5
Trench bottom	8.3	19.7	10.8	21.3	21.6	27.8
Offshore surface	2.3	11.6	2.2	9.9	4.4	11.5
Offshore bottom	4.7	16.7	5.9	17.2	10.3	16.2
Inner western	3.8	16.2	4.2	18.8	6.0	21.2
Outer western	2.2	14.6	2.2	12.4	4.9	14.3

from photosynthesis-irradiance experiments (Lehrter et al., 2009). Model initial conditions were based on the September 2005 cruise data (Murrell et al., 2013b). Field data were averaged by station, ArcGIS (ESRI, 2009) kriging was used to interpolate values across the model grid, and zonal statistics were used to calculate a value for each model grid cell.

Sediment fluxes of ammonium, soluble reactive phosphorus, and dissolved silica were specified in the model based on LCS measurements from 2005 to 2007 (Lehrter et al., 2012) and one cruise in 2010, with the exception of Si which was not available from the 2010 cruise (Lehrter, unpublished). Spatial patterns of ammonium fluxes have been observed in these data with higher fluxes inshore and lower fluxes offshore. A value of 25 mg N m^{-2} d^{-1} was used for the region close to the Atchafalaya and Mississippi rivers. For the mid-depth regions (20–40 m) values between 5 and 8 mg N m^{-2} d^{-1} were used, and at depth deeper than 40 m values of less than 1 mg m^{-2} d^{-1} were used. Soluble reactive phosphorus sediment fluxes range between −0.47 to +2.57 mg P m^{-2} d^{-1}. A constant value of 96 mg Si m^{-2} d^{-1} was used for dissolved silica fluxes.

The GoMDOM grid open boundary was divided into five areas: inner western and outer western, offshore, trench, and eastern (Fig. 1). Field data from locations at both inside and outside (close to the boundary) the computational grid were used to estimate boundary concentrations. Boundary concentrations were estimated for all the state variables. Measurements from all depths were averaged to determine the western boundary concentrations. For the offshore, trench, and eastern boundary areas, field data were averaged above and below the pycnocline as calculated by Lehrter et al. (2009). Boundary concentrations for the model were generated from field data collected during the April, June, and September 2006 cruises. Values from the April cruise were used to estimate the boundary concentrations for January to May, June cruise values for the June to August period and the September values for the September to December period. If data were not available for an area for a specific time period, averages from other cruise years were used. Table 1 show the boundary concentrations for nitrogen and phosphorus.

3.4. Hydrodynamic forcing

The hydrodynamic forcing for GoMDOM was obtained from NCOM-LCS, a three-dimensional numerical coastal ocean model that covers the LCS (Lehrter et al., 2013). The NCOM-LCS model has a horizontal resolution of approximate 1.9 km × 1.9 km, and the boundary conditions are obtained from the Intra-Americas Seas Nowcast/Forecast System (IASNFS) regional ocean model (Ko et al., 2003, 2008; Ko and Wang, 2014). The NCOM-LCS output were aggregated into the approximately 6 km × 6 km grid cells of GoMDOM. NCOM-LCS provided horizontal and vertical flows, vertical mixing coefficients and water temperature. Upon aggregation to the 6 km scale and to reproduce observed salinity patterns, horizontal diffusion coefficients were required to calculate the dispersive contribution to the horizontal transport of state constituents. The Smagorinsky formulation (Smagorinsky, 1963) was used (Smagorinsky coefficient = 0.25 and turbulent Schmidt number = 0.5) to calculate the horizontal diffusion coefficients. Advective flows from the NCOM-LCS ocean model and the horizontal diffusion coefficients were specified at each open boundary flow face.

4. Model calibration

GoMDOM was calibrated to simultaneously fit the processes measurements such as primary production and the salinity, nutrient, phytoplankton (chlorophyll-a) and dissolved oxygen observations for 2006. Our decision to use this year was driven by the availability of a comprehensive dataset of water, sediment and process measurements. However, 2006 was a relatively dry year with an average spring river flow of 18,400 m^3 s^{-1}, which was below the median flow (2000–2014) of 26,700 m^3 s^{-1} and both nitrate + nitrite and total phosphorus spring loads were also below the median loads (http://toxics.usgs.gov/hypoxia/mississippi/fluxests/delivery/, accessed 20.05.15). In contrast, the reported summer hypoxic area of 17,280 km^2 for 2006 was higher than the 20-year median value of 15,587 km^2 (http://www.gulfhypoxia.net, accessed 19.06.15). Spatial regions for averaging field and model results for comparison were identified based on sampling stations and available data from the April, June and September 2006 cruises (Fig. 1). The Mississippi Plume region (region 1) encompassed stations closest to the Mississippi River and is strongly stratified. The average depth is 29.4 m and the median surface and bottom salinities are 20 and 35.8 respectively. The Mississippi Intermediate region (region 2) represented an area near the plume with high rates of primary productivity and was also stratified with the median surface salinity of 29.8 and the bottom salinity of 36. The average depth of this region is 19.9 m. The River Transitions region (region 3) included stations southeast of the Atchafalaya River and west of the Mississippi River plume with an average depth of 16.4 m, and a median surface salinities of 30.0 and a bottom salinity of 35.0. The Outer Continental Shelf plume (region 4) represented the offshore shelf with an average depth of 56.1 m, and a median salinity of 36.5 and no observed surface to bottom salinity gradient. In addition to the regions, station Z01 (depth of 25.3 m), near the Mississippi River plume was chosen for model comparison and analysis (Fig. 1).

Initial model coefficient values were determined based on field measurements in the Gulf of Mexico (Murrell et al., 2013b), results from a one-dimensional model (Pauer et al., 2014), and other estuarine and marine systems (e.g., Cerco and Noel, 2004). A manual approach was used to calibrate the model. Results

Table 2
Table of selected coefficients for GoMDOM model.

Abbreviation	Description	Value	Units
APCP	Phytoplankton P:C ratio	0.0166	–
ANCP	Phytoplankton N:C ratio	0.168	–
BMRD	Diatom base metabolic rate	0.18	d^{-1}
CGZ	Zooplankton maximum growth rate	0.75	d^{-1}
GREFF	Zooplankton grazing efficiency	0.30	–
KDC	DOC mineralization rate (labile fraction)	0.040	d^{-1}
KLC	Hydrolysis rate for labile particulate organic carbon	0.074	d^{-1}
KDN	DON mineralization rate	0.12	d^{-1}
KLN	Hydrolysis rate for labile particulate organic nitrogen	0.060	d^{-1}
KDP	Minimum DOP mineralization rate	0.032	d^{-1}
KLP	Hydrolysis rate for labile particulate organic phosphorus	0.16	d^{-1}
KHND/KHNG	Mean half-saturation constant for nitrogen uptake	0.038	$mg\,L^{-1}$
KHNNT	Half-saturation concentration of ammonium required for nitrification	0.010	$mg\,L^{-1}$
KHP	Half-saturation for algal enhanced mineralization	1.0×10^{-3}	$mg\,L^{-1}$
KHPD/KHPG	Mean half-saturation constant for diatom and non-diatom phosphorus uptake	1.50×10^{-4}	$mg\,L^{-1}$
KSZ	Half-saturation coefficient of zooplankton for phytoplankton	1.05×10^{-5}	$mg\,L^{-1}$
KTGD1/KTGG1	Effect of temperature below optimal temperature for diatoms and non-diatoms	3.5×10^{-3}	$^{\circ}C^{-2}$
KTGD2/KTGG2	Effect of temperature above optimal temperature for diatoms and non-diatoms	0.0	$^{\circ}C^{-2}$
NTM	Nitrification Rate	7.3×10^{-3}	$mg\,L^{-1}\,d^{-1}$
PMD/PMG	Diatom and non-diatom production under optimal conditions	3.9	d^{-1}
SetVel	Settling velocity of particulates	0.25	$m\,d^{-1}$
TMD	Temperature of optimum growth for diatoms	28	$^{\circ}C$
TRD	Metabolism reference temperature for diatoms	25	$^{\circ}C$
ZDTH	Zooplankton death/die-off coefficient	1.2×10^{-7}	$m^3\,d^{-1}\,mg\,C^{-1}$
$P^B{}_{max}$	Maximum production rate per unit biomass	5.00	$g\,C\,(g\,chl\,a\,h)^{-1}$
α (alpha)	Initial slope of the Production-Irradiance (P-I) curve	2.50×10^{-2}	$g\,C\,(g\,chl\,a\,h)^{-1}\,(\mu mol\,quanta\,m^{-2}\,s^{-1})^{-1}$

from one-year simulations were compared to field data for each region. Several hundred runs were performed by varying selected model coefficients. The following skill assessment statistics were used: root mean square error, $RMSE = \sqrt{\Sigma(model - observed)^2/n}$ where n is the number of observations, relative absolute error, $RAE = \Sigma|(model - observed)|/\Sigma(observed)$ and the Spearman correlation coefficient. The set of model coefficients that best matched field observations was considered the final model calibration set of coefficients (see Section 7). Table 2 shows the final model coefficients used in the model.

5. Nitrogen mass budget

The nitrogen and phosphorus masses entering and leaving the model computational grid of the LCS were calculated for 2006. The model was used to calculate the total masses of nitrogen and phosphorus entering and leaving each open boundary (see Fig. 1 for boundaries) based on the specified boundary concentrations and the advective and diffusive boundary exchanges. The model was also used to calculate the amount of nutrient and carbon masses that settled to the bottom and their respective amounts that get recycled back to the water column (see Section 2).

6. Model sensitivity

Using the calibrated model as the base run, sensitivity analyses were performed to investigate the relative importance of the boundary conditions versus the river loads on the water quality of the LCS. Total nitrogen river loads were varied by ±25% and boundary concentrations were varied by ±25% and +10% and model simulations were performed over a 1-year period. Changes in surface and bottom total nitrogen concentration and column integrated primary production in the study area were observed at different regions, and at station Z01 within the study area (Fig. 1). Similarly, total phosphorus river loadings and boundary concentrations were varied by ±25% and the primary production changes in the same locations were observed. Two additional sensitivity simulations were performed: (1) the total phosphorus and total nitrogen river loadings were simultaneously changed by ±25% and (2) the phosphorus and total nitrogen boundary concentrations were simultaneously changed by ±25% and by +10%. Results were analyzed for the months of April, June and September 2006. Sediment sensitivity analyses, similar to the river and boundary sensitivities were also performed by varying the sediment ammonium and soluble reactive phosphorus fluxes by ±25%.

7. Results

The salinity, nutrient, chlorophyll-a and dissolved oxygen field observations at the four regions used for model calibration are summarized in Table 3a. Model output agrees well with the total nitrogen field data (RAE = 0.22) in all four regions (Fig. 2, Table 3b). The model output also demonstrates a reasonable agreement with the total phosphorus (RAE = 0.31), soluble reactive phosphorus (RAE = 0.82), nitrate + nitrite (RAE = 1.06), chlorophyll-a (RAE = 1.10), salinity (RAE = 0.07) and dissolved oxygen (RAE = 0.24) field observations. The Spearman correlation coefficients also show that there is a moderate (0.45) to very strong (0.87) correlation between the model output and the field observations. Modeled primary production compared well with the field observations in regions 2 and 4 (Fig. 3). However, the model slightly under-predicts the spring production in region 1, although within the large range of the observations. The modeled primary production is higher than the observations in region 3 for the spring and summer period. The primary production observations in region 3 were surprisingly low, compared to regions 2 and 4. With the limited observations in region 3 it is unclear whether the mismatch is because of the uncertainty with primary production experiments or some underlying discrepancy with the model.

The total nitrogen mass entering via the boundaries of the computational grid was an order of magnitude greater than the river load, although the net flux was an export from the grid. River

Table 3a
Summary statistics of total nitrogen, phosphorus, soluble reactive phosphorus (SRP) and nitrate + nitrite (NOx) field observations for three 2006 cruises for each of the four regions (see Fig. 1).

		Region 1	Region 2	Region 3	Region 4
Nitrogen (μg/L)	Median	183	243	208	116
	25% percentile	135	183	157	95
	75% percentile	288	301	265	163
Phosphorus (μg/L)	Median	26	24	17	11
	25% percentile	17	16	12	10
	75% percentile	32	40	20	15
SRP (μg/L)	Median	10	4	4	5
	25% percentile	4	2	2	2
	75% percentile	16	31	5	8
NOx (μg/L)	Median	44	40	6	7
	25% percentile	13	6	0	1
	75% percentile	92	73	31	31

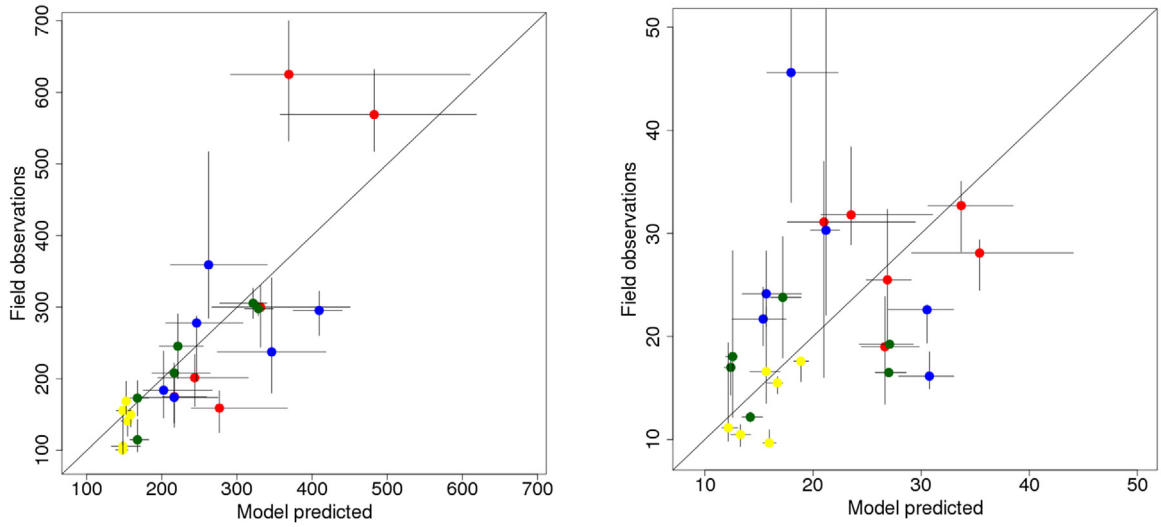

Fig. 2. Model results versus observations (as μg/L) for total nitrogen (left panel) and total phosphorus (right panel). The median surface and median bottom layer field observations for the April, June and September 2006 cruises are shown by the dots while the horizontal and vertical lines represent the modeled and measured ranges, respectively. Red dots = region 1, blue dots = region 2, green dots = region 3 and yellow dots = region 4.

loads dominated the non-boundary total nitrogen input (75%), but still represented only 7.4% of the total nitrogen mass transported into the model grid (Table 4a). Atmospheric deposition was the smallest contributor of total nitrogen mass to the system, at 0.2%. The offshore, trench, and eastern boundaries were the largest total nitrogen sinks. The western boundary has a small net mass of total nitrogen entering the grid. The mass budget for phosphorus was similar to the nitrogen mass budget with the boundaries dominating the mass entering and leaving the study area (Table 4b).

A 25% increase in the boundary total nitrogen concentrations had a greater effect on the total nitrogen concentrations at all regions than the same percent increase in the river loads (Table 5, Appendix 2). Compared to September river loadings, the spring loads more strongly impacted the surface waters of the stratified regions 1 and 2 which are closer to the Mississippi River outlets than the other regions. As expected, the river loads had little impact on region 4, which is farther from the river and closer to the offshore boundary. The total nitrogen concentrations at all four regions on the shelf were more sensitive to changes in river loads during the spring season than during the fall.

A 25% increase in the total nitrogen boundary concentration resulted in a greater increase in primary production than a 25% increase in the total nitrogen river load at all regions (Table 6, Appendix 3). The model results showed that the spring primary production was not very sensitive to changes in total nitrogen boundary concentrations and river loads at regions 1, 2, and 3 with values changing by approximately 5% or less. However, in fall, the primary production in all regions was more sensitive to increased total nitrogen boundary concentrations but responding to a lesser extent to river loads. The overall effect of increases in phosphorus boundary conditions and river loads on primary production was relatively small in the study area. The effect of the 25% increase in phosphorus boundary conditions and river loads on primary production was similar to the same percent increase in total nitrogen, during the spring at regions 1 and 2. During spring for regions 1, 2 and 3, the effect of simultaneously increasing the

Table 3b
Model skill assessment statistics for nitrate + nitrite (N0x), total nitrogen (TN), soluble reactive phosphorus (SRP), total phosphorus (TP), chlorophyll-a, dissolved oxygen (DO) and salinity. n is the sample size (surface and bottom values for three 2006 cruises at the four regions), RMSE is the root mean square error, RAE is the relative absolute error and r_s is the Spearman correlation coefficient.

State variable	n	RMSE	RAE	r_s
NOx	24	58.6	1.06	0.49
TN	24	75.8	0.22	0.87
SRP	24	9.24	0.82	0.45
TP	24	8.76	0.31	0.49
Chlorophyll-a	24	5.65	1.10	0.49
DO	24	1.88	0.24	0.80
Salinity	24	3.32	0.07	0.70

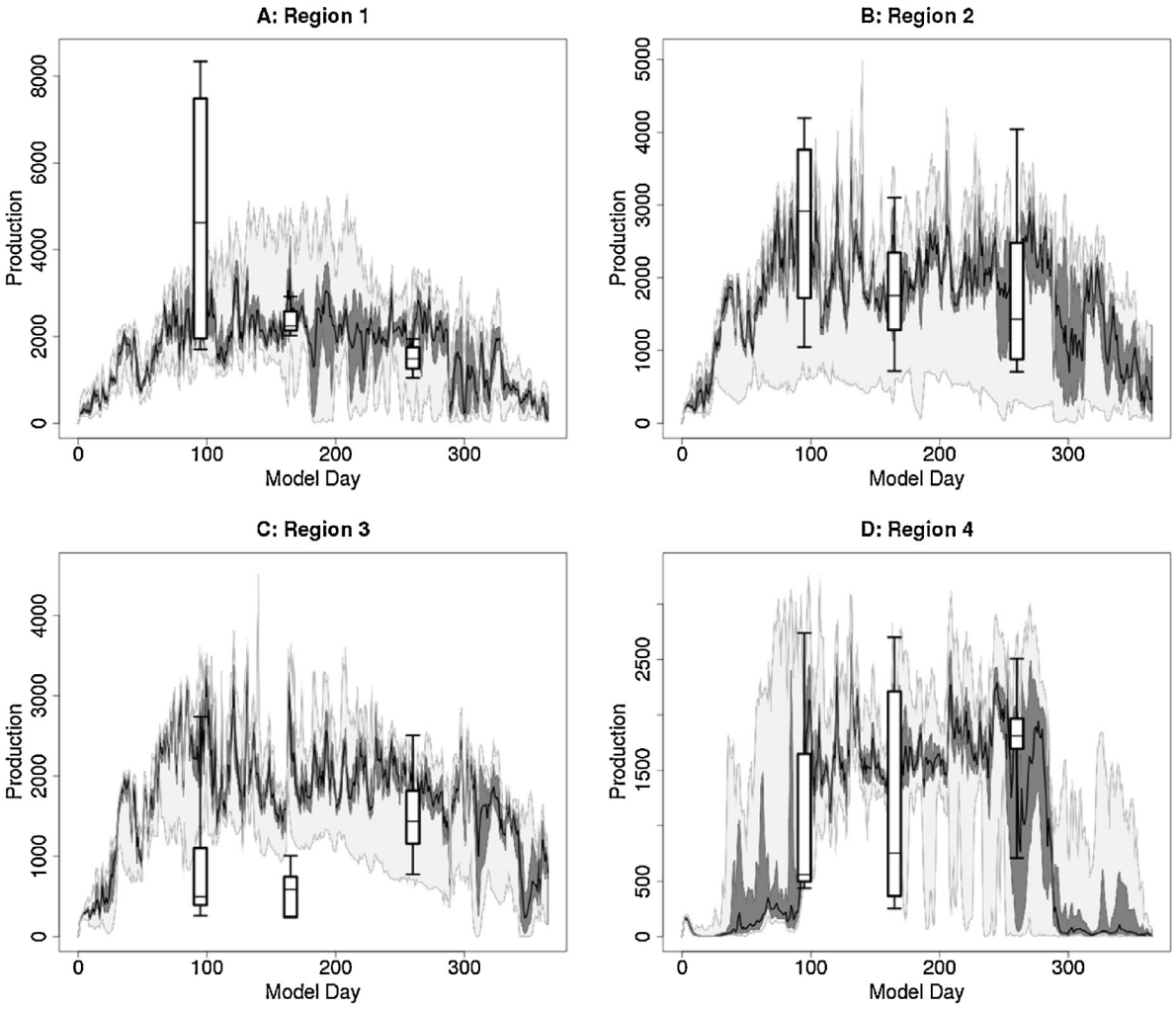

Fig. 3. Time-series plot of modeled versus measured column integrated primary production (expressed as mg C m^{-2} d^{-1}) in regions 1, 2, 3 and 4 for 2006. The field data are shown as Box and Whisker plots (median, 25th and 75th percentiles, minimum and maximum), while the model output is shown as median (black line), 25th to 75th percentile (dark shaded) and minimum to maximum values (light shaded).

Table 4a
Total nitrogen mass entering and exiting the computational grid of the LCS for 2006.

	Mass entering grid (kg)	% of mass entering grid	Mass exiting grid (kg)	% of mass exiting grid	Net mass (kg)
Rivers	9.31×10^8	7.4%	0	0%	9.31×10^8
Sediment	2.71×10^8	2.2%	4.30×10^8	3.5%	-1.59×10^8
Atmosphere	1.97×10^7	0.2%	0	0%	1.97×10^7
Boundaries					
Eastern	2.70×10^9	21.6%	3.03×10^9	24.5%	-3.32×10^8
Trench	2.55×10^9	20.4%	2.61×10^9	21.0%	-5.56×10^7
Offshore	5.07×10^9	40.5%	5.42×10^9	43.7%	-3.46×10^8
Western	9.76×10^8	7.8%	9.22×10^8	7.4%	5.44×10^7
Net mass	$\mathbf{1.25 \times 10^{10}}$	**100%**	$\mathbf{1.24 \times 10^{10}}$	**100%**	$\mathbf{1.13 \times 10^8}$

Table 4b
Total phosphorus mass entering and exiting the computational grid of the LCS for 2006.

	Mass entering grid (kg)	% of mass entering grid	Mass exiting grid (kg)	% of mass exiting grid	Net mass (kg)
Rivers	8.98×10^7	6.7%	0	0%	8.98×10^7
Sediment	6.71×10^6	0.5%	5.54×10^7	4.1%	-4.87×10^7
Atmosphere	0	0%	0	0%	0
Boundaries					
Eastern	3.27×10^8	24.4%	3.54×10^8	26.2%	-2.67×10^7
Trench	2.75×10^8	20.5%	2.77×10^8	20.5%	-1.48×10^6
Offshore	5.34×10^8	39.8%	5.78×10^8	42.8%	-4.38×10^7
Western	1.09×10^8	8.09%	8.75×10^7	6.48%	2.11×10^7
Net mass	$\mathbf{1.34 \times 10^9}$	**100%**	$\mathbf{1.35 \times 10^9}$	**100%**	$\mathbf{-9.90 \times 10^6}$

Table 5
Sensitivity analysis showing the impact of a 25% increase in the total nitrogen boundary concentrations and a 25% increase in river loads on the total nitrogen concentration of the four regions as compared to the base run.

		Region 1		Region 2		Region 3		Region 4	
		Surface	Bottom	Surface	Bottom	Surface	Bottom	Surface	Bottom
April	Boundary +25%	12.4%	18.2%	12.4%	15.5%	14.6%	14.6%	21.8%	21.8%
	River load +25%	9.1%	2.7%	9.1%	5.0%	6.6%	5.6%	0.1%	0.0%
Sept	Boundary +25%	18.2%	21.9%	16.6%	18.6%	16.7%	16.7%	21.9%	22.3%
	River load +25%	4.8%	1.0%	4.9%	4.5%	6.3%	5.0%	0.6%	0.2%

Table 6
Sensitivity analysis of a 25% increase in total nitrogen (TN), phosphorus (P) and combined nitrogen and phosphorus (N&P) in the boundary concentrations and river loads on the column integrated primary production at the four regions as compared to the base run.

		Region 1	Region 2	Region 3	Region 4
April	Boundary TN +25%	5.1%	2.3%	<1%	22.5%
	River load TN +25%	2.7%	<1%	<1%	<1%
September	Boundary TN +25%	16.1%	11.4%	13.0%	82.1%
	River load TN +25%	7.3%	3.4%	3.8%	3.6%
April	Boundary P +25%	4.3%	6.8%	<1%	<1%
	River load P +25%	2.6%	3.1%	<1%	<1%
September	Boundary P +25%	0.2%	2.0%	1.1%	<1%
	River load P +25%	<1%	<1%	<1%	<1%
April	Boundary TN & P +25%	11.1%	10.4%	8.4%	22.5%
	River load TN & P +25%	6.3%	2.7%	2.0%	<1%
September	Boundary TN & P +25%	16.7%	17.4%	16.4%	80.1%
	River load TN & P +25%	7.2%	4.2%	3.4%	2.7%

total nitrogen and phosphorus boundary concentrations on primary production was larger than the effect of increasing only the total nitrogen boundary concentrations. This was not the case at region 4 in the spring or at any regions in the fall. Varying ammonium and soluble reactive phosphorus sediment fluxes (data not shown here) had a small impact on primary production at all the regions for the entire year. The biggest impact was a 3.5% change during September in region 3 but in most cases it was less than 1%.

8. Discussion

GoMDOM was able to represent nutrient and primary production observations in the LCS during 2006. We therefore believe that this numerical model has the skill to calculate nutrient mass budgets and perform model sensitivity experiments, and that the results can provide insight into nutrient and primary production dynamics on the shelf.

Although the boundary exchanges are a net export, fluxes across the large open boundaries comprise the majority of the total nitrogen mass entering the grid (Table 4a). In contrast, the rivers contribute less than 10% of the total nitrogen mass entering the grid. Given the large total nitrogen boundary fluxes, it is not surprising that the total nitrogen concentrations in our study area of the LCS were generally more sensitive to an increase in total nitrogen boundary concentrations than to an increase in total nitrogen river loads (Table 5). However, the relative sensitivity of the total nitrogen concentrations within the study area was influenced by spatial location, depth (surface or bottom waters) and season. Both the surface and bottom layers of region 4, the farthest region from the rivers, were mainly influenced by the boundary conditions. In contrast, the surface waters of regions 1 and 2 and station Z01, which are relatively far away from the boundaries and closer to the river discharges (Fig. 1), were strongly affected by both the boundary concentrations and river loads (Table 5, Appendix 2). Riverine total nitrogen loading had a larger effect on the total nitrogen concentrations during spring than in fall (Table 5). The fall total nitrogen concentrations were less influenced by the river loads because of a period of low river flows resulting in small total nitrogen loading to the study area as well as seasonal reversals in the coastal current (Cochrane and Kelly, 1986), which lessen the effect of river loads on the LCS during late-summer and fall. The spring (April–June) river total nitrogen load is roughly five times higher than the load in fall (Battaglin et al., 2010; Aulenbach et al., 2007). In contrast, the boundary concentrations seem to impact the system for all periods analyzed and likely for the entire year. It should be noted that the analysis was done using river flows and nutrient loads for 2006 which was a relatively dry year with below average nutrient loads (http://toxics.usgs.gov/hypoxia/mississippi/flux_ests/delivery/, accessed 20.05.15). It is therefore possible that riverine nutrients have a larger impact on the LCS during years with average and above average precipitation.

In contrast to the total nitrogen concentration sensitivity to the boundaries (Table 5), spring column-integrated primary production was less sensitive to increased boundary total nitrogen concentration (Table 6) at regions 1, 2 and 3. Primary production sensitivity to changes in the phosphorus boundary at these three regions was similar to the changes in the total nitrogen boundary concentrations. Primary production in region 4, which is the farthest away from the rivers and close to the open ocean boundary, was very sensitive to changes in the total nitrogen boundary concentration. Primary productivity in regions 1, 2 and 3 was also sensitive to changes in the total nitrogen boundary concentration during September. The strong response of fall (September) primary production to increased total nitrogen boundary concentration is likely due to nitrogen limitation as a result of the depletion of high spring nitrogen concentrations on the shelf throughout the summer. In sharp contrast, the model showed that primary production in all the regions of our study area displayed very little sensitivity to changes in the phosphorus boundary concentrations during September.

Increasing the total nitrogen and phosphorus boundary concentrations simultaneously resulted in a much larger increase in primary production in April at regions 1, 2 and 3 compared to increases in either total nitrogen or phosphorus boundary concentrations (Table 6). The results indicate that primary production in these regions is likely nutrient (nitrogen and phosphorus) co-limited in spring. During the spring period, large total nitrogen loads from the rivers are discharged to the LCS resulting in high total nitrogen concentrations relative to phosphorus. The high total nitrogen concentrations on the shelf cause a shift from nitrogen limitation to phosphorus limitation or co-limitation. This interpretation is supported by previous observations and models in the LCS (Laurent et al., 2012; Quigg et al., 2011; Sylvan et al., 2006). However, Turner and Rabalais (2013) concluded that phosphorus limitation alone is uncommon and, when it does occur, is usually accompanied by nitrogen co-limitation. In our model, primary production in region 4 increased as a result of increasing both total nitrogen and phosphorus boundary concentrations similar to the impact of increased total nitrogen boundary concentrations alone, indicating that this region is nitrogen limited for most of the year. Also, increasing the phosphorus and total nitrogen boundary concentrations resulted in a similar impact on primary production in September for regions 1, 2 and 3 in comparison to increasing only total nitrogen boundary concentrations, indicating that these regions are nitrogen limited in September.

The large amount of nutrients entering the shelf from the boundaries, and its impact on the nutrient regime and primary production, is not surprising given the large surface area of the open boundaries (Fig. 1). However, we have shown that fluxes across the boundaries represent a net nutrient sink, and nutrient concentrations outside the grid are generally lower (Tables 1a and 1b) in comparison with nutrient concentrations on the shelf, especially in the plume area (Fig. 2, Table 3a). Thus, the boundary nutrient fluxes often can have a dilution effect on the shelf nutrient concentrations and the extent of the dilution depends on the concentrations of these nutrient boundary fluxes. Circulation patterns on the shelf for most of the year is generally westward, while the flow is usually reversed in the summer and tend to be in an easterly direction (Schiller et al., 2011; Wiseman et al., 1997). The eastern and trench boundaries, which might be influenced by the Mississippi River, have relatively high nitrogen concentrations (Fig. 1) and can thus impact production on the shelf during the summer months.

It is unclear whether the study area of the LCS would experience a 25% year-to-year fluctuation in nitrogen boundary concentrations, especially the off-shore boundary, but the uncertainty associated with boundary concentration estimates can easily be this high (Table 1). However, even a 10% change in total nitrogen boundary concentration has a very noticeable impact on the nutrient concentrations on the shelf (Appendix 2). The impact of the total nitrogen boundary concentrations on primary production is also influenced by several factors such as the potential for phosphorus limitation, distance from the plume, time of the year, and perhaps wet versus dry years, which can cause the shift between nitrogen and phosphorus limitation or co-limitation.

The selection of the model computational grid was largely driven by data availability to define the initial and boundary concentrations for the nutrients and other model state variables. However, a limitation of our model grid is that the boundaries, especially the eastern boundary, can still be influenced by the MARB and thus have a relatively large impact on predicted shelf production. Expanding the computational grid and moving the boundaries, especially the eastern and trench boundaries, farther away from the MARB influence will likely decrease the impact of the boundaries on shelf production. However, expanding model grids requires addressing nutrient sources from additional rivers to the east and west of our current grid and the potential for nutrient upwelling from the eastern canyon (Fig. 1). A larger computational grid also increases computer resources and requires additional sampling (which is already limited) to estimate boundaries and initial conditions for an extended study area.

Other modeling efforts have dealt with the lack of spatial and seasonal measurements to estimate nutrient boundary conditions in different ways. Fennel et al. (2011) and Laurent and Fennel (2014) have used nutrient climatological data from the World Ocean Database (Boyer et al., 2006). However, the nutrient climatological data is currently only available at $1^\circ \times 1^\circ$ resolution, which is spatially coarse for the continental shelf, and the climatological data only contain inorganic nitrogen and phosphorus concentrations. In contrast, it has been observed that organic nitrogen and phosphorus inputs to the LCS from offshore can exceed the organic N and P inputs from the Mississippi River (Lehrter et al., 2013). Justić and Wang (2014) used numerical methods to estimate nutrient boundaries. A limitation of this approach is that the boundary impacts are disconnected from observations made outside the computational grid. Thus the model does not have the ability to investigate the impact of changes in boundary concentrations (such as our study) on the primary production on the shelf.

The results from this modeling study demonstrate the importance of nutrient boundaries on primary production on the LCS. We believe that it is important for any future modeling studies to conduct field measurements in order to obtain accurate spatial and seasonal nutrient boundaries. It will also be beneficial to perform sensitivity analyses (similar to this study) to understand and quantify the impact of the nutrient boundaries on the shelf nutrient regime and primary production. In a follow-up paper (Feist et al., in preparation) we will extend this analysis to address the influence of cross boundary fluxes when predicting hypoxic area under different MARB nutrient load reduction scenarios.

Acknowledgements

The work was funded entirely by the US Environmental Protection Agency. We thank Mark Rowe for the thorough review of the manuscript and his constructive comments, and Dave Griesmer and Ken Rygwelski for helping with the graphics. The views expressed in this paper are those of the authors and do not necessarily reflect the views or policies of the U.S. Environmental Protection Agency.

Appendix 1. Calculation of the light attenuation coefficient, k_d

Water quality data including salinity, a proxy for colored dissolved organic matter from the rivers, chlorophyll and organic carbon, and light profiles used to generate the light attenuation equation were collected during six cruises from 2005 to 2007. Photosynthetically active radiation (PAR) was measured continuously during the cruises by a shipboard LICOR 2π LI-190 irradiance sensor and logged at 15 min intervals to a LICOR LI-1000 logger. A value for k_d was calculated for each cell of the computational grid using the Beer equation (see Equation 3 in the paper). Samples within an initial light below 75 μmol E/m^2 s were not included in this analysis. The resulting non-normal k_d values were transformed using a Box–Cox transformation with $\lambda = -0.10$ to normalize distribution. The water column characteristics were also transformed. The full dataset was divided into three independent groups through random selection: a calibration set of 259 points and two verification sets of 65 points each. A multiple linear regression was performed using salinity (S), chlorophyll (Phyto, in units of μg/L) and non-phytoplankton particulate organic carbon (PartC in unit of mg L^{-1}). The full equation, including the reversal of the initial

Box–Cox transformation, is presented in the equation below,

$$k_d = (-0.10 \cdot [-0.5606 - 1.084 \times 10^{-6} \cdot S^4 + 0.2085 \cdot \ln(\text{Phyto}) + 0.7640 \cdot \sqrt{(\text{PartC})}] + 1)^{1/-0.10}$$

The R^2 for the calibration data set was 0.68, while the verification sets had R^2 values of 0.69 and 0.71. The slope of the verification sets were 1.09 and 1.01, suggesting that the independent data sets produced a relationship that did not deviate more than 10% from the 1:1 line. Salinity was the most important factor in the regression, and exhibited the highest influence on the attenuation coefficient. Chlorophyll was second in importance. Non-phytoplankton carbon material was considered significant, but had the least influence on k_d. Non-phytoplankton carbon is represented by zooplankton, labile organic carbon, and refractory organic carbon in the model.

Appendix 2. Total nitrogen (TN) concentration and percent change in TN concentration from a base run by region in response to increased or decreased river load or boundary TN concentration.

Nitrogen	Base Run	Boundary +25% TN		Boundary −25% TN		River +25% TN		River −25% TN		Boundary +10% TN	
	mg m^{-3}	mg m^{-3}	% Change	mg m^{-3}	% Change	mg m^{-3}	% Change	mg m^{-3}	% Change	mg m^{-3}	% Change
April											
Reg 1 – Surf	398	448	12.4	349	−12.3	434	9.1	363	−8.8	418	5.0
Reg 1 – Bot	276	327	18.2	226	−18.2	284	2.7	269	−2.7	297	7.3
Reg 2 – Surf	385	433	12.4	338	−12.4	420	9.1	351	−8.9	404	5.0
Reg 2 – Bot	327	378	15.5	277	−15.4	343	5.0	311	−4.8	347	6.2
Reg 3 – Surf	312	357	14.6	267	−14.3	332	6.6	291	−6.6	330	5.8
Reg 3 – Bot	308	352	14.6	263	−14.4	325	5.6	291	−5.4	326	5.9
Reg 4 – Surf	150	183	21.8	117	−22.0	151	0.1	150	−0.1	164	8.8
Reg 4 – Bot	158	192	21.8	125	−21.0	158	0.0	158	0.0	171	8.6
Z01 – Surf	513	560	9.1	466	−9.3	579	12.9	446	−13.0		
Z01 – Bot	345	395	14.4	295	−14.5	368	6.53	322	−6.7		
June											
Reg 1 – Surf	301	342	13.4	262	−13.0	331	9.9	274	−9.1	317	5.3
Reg 1 – Bot	246	292	18.5	200	−18.8	252	2.3	240	−2.5	264	7.5
Reg 2 – Surf	273	310	13.6	236	−13.6	298	9.0	247	−9.5	288	5.4
Reg 2 – Bot	228	269	17.8	188	−17.7	236	3.2	222	−2.8	244	7.1
Reg 3 – Surf	225	259	15.4	192	−14.6	245	9.0	204	−8.8	239	6.2
Reg 3 – Bot	227	261	15.3	192	−15.5	239	5.4	213	−6.0	241	6.2
Reg 4 – Surf	145	174	20.2	115	−20.3	148	2.4	141	−2.6	156	8.0
Reg 4 – Bot	147	180	22.1	115	−21.8	147	0.1	147	−0.1	160	8.8
Z01–Surf	424	458	8.0	388	−8.4	483	13.9	362	−14.7		
Z01 – Bot	291	336	15.5	245	−15.72	306	5.0	274	−6.0		
September											
Reg 1 – Surf	257	304	18.1	211	−18.0	270	4.8	245	−4.5	276	7.4
Reg 1 – Bot	230	281	21.9	180	−21.9	232	1.0	228	−1.0	251	8.8
Reg 2 – Surf	246	287	16.6	205	−16.8	258	4.9	232	−5.8	263	6.7
Reg 2 – Bot	235	279	18.6	194	−17.4	246	4.5	227	−3.7	253	7.3
Reg 3 – Surf	187	218	16.7	160	−14.3	199	6.3	174	−7.2	200	6.6
Reg 3 – Bot	186	216	16.7	159	−14.5	195	5.0	173	−6.8	198	6.8
Reg 4 – Surf	128	156	21.9	100	−21.9	129	0.6	127	−0.6	139	8.8
Reg 4 – Bot	154	189	22.3	121	−22.1	155	0.2	155	−0.2	169	8.9
Z01 – Surf	328	376	14.7	274	−16.3	348	6.1	300	−8.3		
Z01 – Bot	251	298	18.7	205	−18.6	260	3.5	243	−3.4		

Reg refers to the model region, Surf = surface, Bot = bottom.

Appendix 3.1. Column-integrated primary production and change in column-integrated primary production (mg C m^{-2} d^{-1}) from a base run in response to increased or decreased river load and boundary total nitrogen (TN) concentrations.

	Base run	Boundary +25% TN		Boundary −25% TN		River +25% TN		River −25% TN		Boundary +10% TN	
	Value	Value	% Change	Value	% Change	Value	% Change	Value	% Change	Value	% Change
April											
Region 1	2190	2301	5.1	2031	−7.3	2247	2.7	2083	−4.9	2240	2.3
Region 2	2136	2185	2.3	2029	−5.0	2147	0.5	2107	−1.4	2170	1.6
Region 3	2094	2113	0.9	1895	−9.5	2111	0.8	2053	−2.0	2117	1.1
Region 4	1482	1815	22.5	1127	−23.9	1484	0.2	1478	−0.2	1619	9.2
June											
Region 1	2354	2459	4.5	2165	−8.0	2447	4.0	2165	−8.0	2405	2.2
Region 2	1812	1865	2.9	1712	−5.5	1842	1.6	1761	−2.8	1832	1.1
Region 3	1746	1746	0.0	1684	−3.5	1755	0.6	1726	−1.1	1750	0.2
Region 4	1482	1818	17.5	1220	−21.1	1592	2.9	1501	−2.9	1674	8.2
Sept											
Region 1	1904	2210	16.1	1547	−18.7	2043	7.3	1750	−8.1	2030	6.6
Region 2	2112	2354	11.4	1786	−15.4	2185	3.4	1999	−5.4	2218	5.0
Region 3	1698	1919	13.0	1437	−15.4	1762	3.8	1625	−4.3	1793	5.6
Region 4	786	1432	82.1	204	−74.0	814	3.6	753	−4.2	1044	32.8

Appendix 3.2. Column-integrated primary production and change in column-integrated primary production (mg C m^{-2} d^{-1}) from a base run in response to increased or decreased river load and boundary phosphorus (P) concentrations.

	Base run	Boundary +25% P		Boundary −25% P		River +25% P		River −25% P	
	Value	Value	% Change	Value	% Change	Value	% Change	Value	% Change
April									
Region 1	2190	2283	4.3	2001	−8.6	2245	2.6	2104	−3.9
Region 2	2136	2281	6.8	1841	−13.8	2201	3.1	2080	−2.6
Region 3	2094	2096	0.1	1772	−15.4	2106	0.6	2073	−1.0
Region 4	1482	1482	0.0	1483	0.1	1481	0.0	1482	0.0
June									
Region 1	2354	2485	5.6	2086	−11.4	2423	3.0	2268	−3.6
Region 2	1812	1992	10.0	1585	−12.5	1845	1.8	1779	−1.8
Region 3	1746	1935	10.1	1478	−15.3	1778	1.9	1718	−1.6
Region 4	1482	1543	−0.2	1469	−5.0	1538	−0.6	1555	0.6
Sept									
Region 1	1904	1907	0.2	1896	−0.4	1904	0.0	1900	−0.2
Region 2	2112	2155	2.0	1974	−6.5	2111	−0.1	2089	−1.1
Region 3	1698	1716	1.1	1601	−5.7	1685	−0.8	1712	−0.8
Region 4	786	778	−1.1	806	2.5	780	−0.8	794	1.0

Appendix 3.3. Column-integrated primary production (mgC m^{-2} d^{-1}) and change in column-integrated primary production from a base run in response to increased or decreased river load and boundary concentrations of combined phosphorus (P) and total nitrogen (TN).

	Base run	Boundary +25% P, TN		Boundary −25% P, TN		River +25% P, TN		River −25% P, TN		Boundary +10% P, TN	
	Value	Value	% Change	Value	% Change	Value	% Change	Value	% Change	Value	% Change
April											
Region 1	2190	2433	11.1	1912	−12.7	2327	6.3	2025	−7.5	2294	4.8
Region 2	2136	2358	10.4	1800	−15.7	2194	2.7	2061	−3.5	2243	5.0
Region 3	2094	2268	8.4	1793	−14.4	2194	2.0	2044	−2.4	2176	3.9
Region 4	1482	1815	22.5	1128	−23.9	1484	0.2	1478	−0.2	1619	9.3
June											
Region 1	2354	2686	14.1	2010	−14.6	2567	9.1	2138	−9.2	2487	5.7
Region 2	1812	2092	15.4	1534	−15.3	1883	3.9	1742	−3.9	1917	5.8
Region 3	1746	2002	14.7	1479	−15.3	1795	2.8	1694	−3.0	1847	5.8
Region 4	1547	1880	21.6	1233	−20.3	1587	2.6	1513	−2.2	1683	8.8
Sept											
Region 1	1904	2222	16.7	1553	−18.4	2042	7.2	1752	−8.0	2030	6.6
Region 2	2112	2480	17.4	1734	−17.9	2200	4.2	1998	−5.4	2254	6.9
Region 3	1698	1976	16.4	1409	−17.0	1755	3.4	1640	−3.4	1811	6.7
Region 4	786	1416	80.1	217	−72.4	808	2.7	764	−2.8	1039	32.1

References

Aulenbach, B.T., Buxton, H.T., Battaglin, W.A., Coupe, R.H., 2007. Streamflow and Nutrient Fluxes of the Mississippi-Atchafalaya River Basin and Subbasins for the Period of Record Through 2005. U.S. Geological Survey Open-File Report 2007-1080.

Banas, N.S., Lessard, E.J., Kudela, R.M., MacCready, P., Peterson, T.D., Hickey, B.M., Frame, E., 2009. Planktonic growth and grazing in the Columbia River plume region: a biophysical model study. J. Geophys. Res. 114, http://dx.doi.org/10.1029/2008JC004993.

Battaglin, W.A., Aulenbach, B.T., Vecchia, A., Buxton, H.T., 2010. Changes in Streamflow and the Flux of Nutrients in the Mississippi-Atchafalaya River Basin, USA, 1980–2007. U.S. Geological Survey Scientific Investigations Report 2009-5164., pp. 47.

Bianchi, T.S., DiMarco, S.F., Cowan, J.H., Hetland, R.D., Chapman, P., Day, J.W., Allison, M.A., 2010. The science of hypoxia in the Northern Gulf of Mexico: a review. Sci. Total Environ. 408, 1471–1484.

Bierman Jr., V.J, Hinz, S.C., Zhu, D-W., Wiseman, W.J., Rabalais, N.N., Turner, R.E., 1994. A preliminary mass balance model of primary productivity and dissolved oxygen in the Mississippi River plume/inner Gulf shelf region. Estuaries 17, 886–899.

Breed, G.A., Jackson, G.A., Richardson, T.L., 2004. Sedimentation, carbon export and food web structure in the Mississippi River plume described by inverse analysis. Mar. Ecol. Prog. Ser. 278, 35–51.

Boyer, T.P., Antonov, J.I., Garcia, H.E., Johnson, D.R., Locarnini, R.A., Mishonov, A.V., Pitcher, M.T., Baranova, O.K., Smolyar, I.V., 2006. World ocean database 2005. In: Levitus, S. (Ed.), NOAA Atlas NESDIS 60. U.S. Government Printing Office, Washington, D.C., p. 190, DVDs.

Byun, D.W., Schere, K.L., 2006. Review of the governing equations, computational algorithms and other components of the models-3 Community Multiscale Air Quality (CMAQ) modeling system. Appl. Mech. Rev. 59, 51–77.

Cerco, C., Meyers, M., 2000. Tributary refinements to the Chesapeake Bay Model. J. Environ. Eng. 126, 164–174.

Cerco, C., Noel, M., 2004. The 2004 Chesapeake Bay Eutrophication Model. Chesapeake Bay Program Office, US Environmental Protection Agency, Annapolis, MD, EPA/903/R/04/004.

Chen, X., Lohrenz, S.E., Wiesenburg, D.A., 2000. Distribution and controlling mechanisms of primary production on the Louisiana–Texas continental shelf. J. Mar. Syst. 25, 179–207.

Cochrane, J.D., Kelly, F.J., 1986. Low-frequency circulation on the Texas-Louisiana continental shelf. J. Geophys. Res. 91 (10), 645–659.

Dagg, M.J., Bianchi, T.S., Breed, G.A., Cai, W.J., Duan, S., Liu, H., McKee, B.A., Powell, R.T., Stewart, C.M., 2005. Biogeochemical characteristics of the lower Mississippi River, USA, during June 2003. Estuaries 28, 664–674.

ESRI (Environmental Systems Resource Institute), 2009. ArcGIS Desktop 9.3. ESRI, Redlands, CA, USA.

Fennel, K., Hetland, R., Feng, Y., DiMarco, S., 2011. A coupled physical-biological model of the Northern Gulf of Mexico shelf: model description, validation and analysis of phytoplankton variability. Biogeosciences 8, 1881–1899.

Feist T.J., Pauer J.J., Melendez W., Lehrter J.C., DePetro P.A., Rygwelski K.R. Evaluating the relative importance of nutrient and organic carbon loads, boundary fluxes, and sediment fluxes on hypoxia in the northern Gulf of Mexico using a biogeochemical model (in preparation).

Fry, B., Justic, D., Riekenberg, P., Swenson, E., Turner, R., Wang, L., Pride, L., Rabalais, N., Kurtz, J., Lehrter, J., Murrell, M., Shadwick, E., Boyd, B., 2015. Carbon dynamics on the Louisiana continental shelf and cross-shelf feeding of hypoxia. Estuaries Coasts 38 (3), 703–721.

Green, R.E., Breed, G.A., Dagg, M.J., Lohrenz, S.E., 2008. Modeling the response of primary production and sedimentation to variable nitrate loading in the Mississippi River plume. Cont. Shelf Res. 28, 1451–1465.

Hodur, R.M., 1997. The naval research laboratory's coupled ocean/atmosphere mesoscale prediction system (COAMPS). Mon. Weather Rev. 125, 1414–1430.
Jassby, A.D., Platt, T., 1976. Mathematical formulation of the relationship between photosynthesis and light for phytoplankton. Limnol. Oceanogr. 21, 540–547.
Justić, D., Wang, L., 2014. Assessing temporal and spatial variability of hypoxia over the inner Louisiana–upper Texas shelf: application of an unstructured-grid three-dimensional coupled hydrodynamic-water quality model. Cont. Shelf Res. 72, 163–179.
Ko, D.S., Preller, R.H., Martin, P.J., 2003. An experimental real-time intra Americas sea ocean nowcast/forecast system for coastal prediction. In: Proceedings, AMS 5th Conference on Coastal Atmospheric & Oceanic Prediction & Processes, http://www.7320.nrlssc.navy.mil/IASNFS_WWW/IASNFS_intro.html.
Ko, D.S., Martin, P.J., Rowley, C.D., Preller, R.H., 2008. A real-time coastal ocean prediction experiment for MREA04. J. Mar. Syst. 69, 17–28.
Ko, D.S., Wang, D.P., 2014. Intra-Americas Sea Nowcast/Forecast System Ocean Reanalysis to Support Improvement of Oil-Spill Risk Analysis in the Gulf of Mexico by Multi-Model Approach, Bureau of Ocean Energy Management Report 2014-1003., pp. 55.
Laurent, A., Fennel, K., Hu, J., Hetland, R., 2012. Simulating the effects of phosphorus limitation in the Mississippi and Atchafalaya River plumes. Biogeosciences 9, 4707–4723.
Laurent, A., Fennel, K., 2014. Simulated reduction of hypoxia in the northern Gulf of Mexico due to phosphorus limitation. Elementa: Sci. Anthr. 2, 1–12.
Le, C., Lehrter, J.C., Hu, C., Murrell, M.C., Qi, L., 2014. Spatiotemporal chlorophyll – a dynamics on the Louisiana continental shelf derived from a dual satellite imagery algorithm. J. Geophys. Res.: Oceans 119, 7449–7462.
Lehrter, J.C., Murrell, M.C., Kurtz, J.C., 2009. Interactions between freshwater input, light, and phytoplankton dynamics on the Louisiana continental shelf. Cont. Shelf. Res. 29, 1861–2187.
Lehrter, J.C., Beddick Jr., D.L., Devereux, R., Yates, D.F., Murrell, M.C., 2012. Sediment-water fluxes of dissolved inorganic carbon, O_2, nutrients, and N_2 from the hypoxic region of the Louisiana continental shelf. Biogeochemistry 109, 233–252.
Lehrter, J.C., Ko, D.S., Murrell, M.C., Hagy III, J.D., Schaeffer, B.A., Greene, R.M., Gould, R.W., Penta, B., 2013. Nutrient distributions, transport pathways, and fate on the inner margin of a river-dominated continental shelf. J. Geophys. Res.: Oceans 118, 4822–4838.
Liu, H., Dagg, M., 2003. Interactions between nutrients, phytoplankton growth, and micro- and mesozooplankton grazing in the plume of the Mississippi River. Mar. Ecol. Prog. Ser. 258, 31–42.
Lohrenz, S.E., Redalje, D.G., Cai, W.J., Acker, J., Dagg, M.J., 2008. A retrospective analysis of nutrients and phytoplankton productivity in the Mississippi River Plume. Cont. Shelf Res. 28, 1466–1475.
Melendez, W., Settles, M., Pauer, J., 2009. LM3: A High Resolution Lake Michigan Mass Balance Water Quality Model. U.S. Environmental Protection Agency, Office of Research and Development, National Health and Environmental Effects Research Laboratory, Mid-Continent Ecology Division-Duluth, Large Lakes Research Station, Grosse Ile, MI, 618 EPA/600/R-09/020.
Murrell, M.C., Lehrter, J.C., 2011. Sediment and lower water column oxygen consumption in the seasonally hypoxic region of the Louisiana continental shelf. Estuaries Coast 34, 912–924.
Murrell, M.C., Stanley, R.S., Lehrter, J.D., Hagy III, J.D., 2013a. Plankton community respiration, net ecosystem metabolism, and oxygen dynamics on the Louisiana continental shelf: implications for hypoxia. Cont. Shelf Res. 52, 27–38.
Murrell, M.C., Aukamp, D.L., Beddick Jr., D.L., Devereux, R., Greene, R.M., Hagy III, J.D., Jarvis, B.M., Kurtz, J.C., Lehrter, J.C., Yates, D.F., 2013b. Gulf of Mexico Hypoxia Research Program Data Report: 2002–2007. Report No. EPA/600/R-13/257. U.S. Environmental Protection Agency, Washington, DC.
National Marine Fisheries Service/Marine Ecosystem Division (NMFS), 2005. Coastal and Oceanic Plankton Ecology Production, and Observation (COPEPOD) Database, Zooplankton carbon mass data, Retrieved from: http://www.st.nmfs.noaa.gov/plankton/2005/biomass-fields.html.
Pauer, J.J., Anstead, A.M., Melendez, W., Rossmann, R., Taunt, K.W., Kreis Jr., R.G., 2008. The Lake Michigan eutrophication model, LM3-Eutro: model development and calibration. Water Environ. Res. 80, 853–861.
Pauer, J.J., Anstead, A.M., Melendez, W., Taunt, K.W., Kreis Jr., R.G., 2011. Revisiting the Great Lakes Water Quality Agreement phosphorus targets and predicting the trophic status of Lake Michigan. J. Great Lakes Res. 37, 26–32.
Pauer, J.J., DePetro, P.A., Anstead, A.M., Lehrter, J.C., 2014. Application of a one-dimensional model to explore the drivers and lability of carbon in the northern Gulf of Mexico. Ecol. Model. 294, 59–70.
Quigg, A., Sylvan, J.B., Gustafson, A.B., Fisher, T.R., Oliver, R.L., Tozzi, S., Ammerman, J.W., 2011. Going west: nutrient limitation of primary production in the Northern Gulf of Mexico and the importance of the Atchafalaya River. Aquat. Geochem. 17, 519–544.
Rabalais, N.N., Turner, R.E., Wiseman Jr., W.J., 2002. Gulf of Mexico hypoxia, AKA 'The dead zone'. Ann. Rev. Ecol. Syst. 33, 235–263.
Rosmond, T.E., Teixeira, J., Peng, M., Hogan, T.F., Pauley, R., 2002. Navy Operational Global Atmospheric Prediction System (NOGAPS): forcing for ocean models. Oceanography 15, 99–108.
Sahl, L.E., Merrell, W.J., Biggs, D.C., 1993. The influence of advection on the spatial variability of nutrient concentrations on the Texas-Louisiana continental shelf. Cont. Shelf Res. 13, 223–251.
Schiller, R.V., Kourafalou, V.H., Hogan, P., Walker, N.D., 2011. The dynamics of the Mississippi River plume: Impact of topography, wind, and offshore forcing on the fate of plume waters. J. Geophys. Res. 116, C06029, http://dx.doi.org/10.1029/2010JC006883.
Smagorinsky, J., 1963. General circulation experiments with the primitive equations. I. The Basic Experiment. Mon. Weather Rev. 91, 99–164.
Sutor, M.M., Dagg, M.J., 2008. The effects of vertical sampling resolution on estimates of plankton biomass and rate calculations in stratified water columns. Estuar. Coast Shelf Sci. 78, 107–121.
Sylvan, J.B., Dortch, Q., Nelson, D.M., Maier Brown, A.F., Morrison, W., Ammerman, J.W., 2006. Phosphorus limits phytoplankton growth on the Louisiana shelf during the period of hypoxia formation. Environ. Sci. Technol. 40, 7548–7553.
Turner, R.E., Rabalais, N.N., 2013. Nitrogen and phosphorus phytoplankton growth limitation in the northern Gulf of Mexico. Aquat. Microb. Ecol. 68, 159–169.
United States Geological Survey, 2013. Streamflow and Nutrient Flux of the Mississippi-Atchafalaya River Basin and Subbasins for the Period of Record through 2012, http://toxics.usgs.gov/hypoxia/mississippi/flux_ests/delivery/index.html.
Walsh, J.J., Dieterle, D.A., Meyers, M.B., Müller-Karger, F.E., 1989. Nitrogen exchange at the continental margin: a numerical study of the Gulf of Mexico. Prog. Oceanogr. 23 (4), 245–330.
Wiseman, W.J., Rabalais, N.N., Turner, R.E., Dinnel, S.P., MacNaughton, A., 1997. Seasonal and interannual variability within the Louisiana coastal current: Stratification and hypoxia. J. Mar. Syst. 12, 237–248.